Journal of The Electrochemical Society, **159** (3) H225-H229 (2012)
0013-4651/2012/159(3)/H225/5/$28.00 © The Electrochemical Society

Carrier Transport Study of TMIn-Treated InGaN LEDs by Using Quantum Efficiency and Time-Resolved Electro-Luminescence Measurements

Shih-Wei Feng[a,z] **and Jen-Inn Chyi**[b,*]

[a]*Department of Applied Physics, National University of Kaohsiung, Kaohsiung, Taiwan*
[b]*Department of Electrical Engineering, National Central University, Taiwan; Department of Optics and Photonics, National Central University, Taiwan; and Research Center for Applied Sciences, Academia Sinica, Taiwan*

The aim of this study is to determine the emission and carrier transport characteristics of Trimethylindium (TMIn)-treated InGaN green light emitting diodes (LEDs) by using quantum efficiency and time-resolved electro-luminescence measurements. As TMIn treatment time increased, a more homogeneous indium composition and low V-shaped defect density lead to slightly blue-shifted peak position, narrower spectrum width, and better luminescence efficiency. In addition, the *ns*-scale response time shows efficient carrier injection and carrier transport. The shorter response times of the longer-TMIn-treated LED suggest that a lower V-shaped density is beneficial to carrier injection into the quantum wells and that a slight carrier localization helps carrier recombination. Furthermore, a μ*s*-scale decay time represents inefficient carrier recombination in the active region. The longer the TMIn treatment time, the shorter the response time, the faster the radiative decay rate, and the slower the nonradiative decay rate. With a forward applied voltage, lower V-shaped defect density, un-reduced polarization field, carrier delocalization, and weaker Auger recombination in the TMIn-treated samples lead to the inevitable efficiency droop. The resulting recombination dynamics are correlated with the device characteristics and performance of the TMIn-treated LEDs. The research results provide important information to solve the efficiency droop of LEDs.
 [DOI: 10.1149/2.011203jes]

Manuscript submitted July 6, 2011; revised manuscript received October 24, 2011. Published December 30, 2011.

Light emitting diodes (LEDs) based on the III-V compound semiconductors can be considered the next generation white lighting.[1] White lighting can be produced using either phosphor conversion or mixed red-green-blue LEDs.[1] The phosphor conversion method exhibits a low color rendering index (CRI) and a low efficiency. To achieve the ultimate performance goal of 200 lm/W, white lighting must be achieved by mixed red-green-blue LEDs.[1] Currently, deep green LEDs are inefficient. This is commonly known as the "Green Gap."[2] Much effort has been devoted to overcoming this problem. It was suggested that both reduced threading dislocations and improved polarization control play huge roles in bridging the green gap.[2] Nonpolar III-nitride semiconductors grown along the *m*- and *a*-axes can be used to reduce the quantum-confined Stark Effect (QCSE).[3]

Quality improvement of InGaN/GaN multiple quantum wells (MQWs) as an active layer of LEDs is also crucial to solve the Green Gap. Many factors contributing to the low quality InGaN/GaN MQWs have been proposed: a thermal instability of InN,[4–6] indium surface segregation,[4–6] phase separation,[4–6] a large lattice mismatch between InN and GaN,[7–9] a low miscibility of InN and GaN,[7–9] and a larger number of mis-fit dislocations and V-shaped defects.[10] It was reported that growth interruption between InGaN well and GaN barrier was effective in improving the structure quality of InGaN/GaN MQWs and enhancing the luminescence intensity.[4–6] By introducing growth interruption at high growth temperature, atoms can migrate into the minimum energy sites to approach thermal equilibrium and decomposition of In-rich InGaN leads to a flat InGaN surface. Hence, the quality of the InGaN layer was significantly improved and the defect density was reduced.[4–6] Also, trimethylindium (TMIn) treatment process during the growth interruption of InGaN well to GaN barrier was shown to enhance the internal quantum efficiency and output power of InGaN/GaN green LEDs.[11] These improvements were attributed to the reduced V-shaped defect density, surface smoothing process, and better InGaN/GaN MQW structures. In our previous study, the effects of TMIn treatment time on the emission and carrier dynamic characteristics of InGaN/GaN MQWs were investigated.[12] TMIn treatment suppresses InGaN decomposition and indium aggregation such that more homogeneous indium composition, low V-shaped defect density, higher energy (localized) states, stronger photoluminescence intensity, and smaller decay time were observed. With a longer TMIn treatment time (the TMIn-180 sec sample), the suppressed diffusion of indium atoms leads to a decomposed phase consisting of InN and slightly broad InGaN distribution, leading to a little rough surface morphology and slight carrier localization. However, the effects of TMIn treatment on the emission and carrier transport behavior of InGaN/GaN green LEDs are not well studied.

Quantum efficiency (QE) measurement is a general tool to estimate the performance of LEDs. QE is defined as the average photon energy flux over the stream of carriers passing through the device.[1] However, QE measurement cannot describe carrier dynamic behaviors. On the other hand, time-resolved electroluminescence (TREL) measurement under electrical fast pulse excitation provides important insights into the carrier generation-recombination of LEDs.[13,14] Through the dynamic behavior of EL, the operation mechanisms of LEDs can be explored, including carrier injection, carrier transport, formation of the excited state, and radiative decay of the excited state. The onset of EL is identified as the point at which the leading fronts of hole and electron pulses meet in the device. The onset of EL can be determined by the response time, i.e., the time delay, t_d, between addressing the device with a short voltage pulse and the first appearance of EL.[13,14] The time at which the EL is maximum is the time at which electron and hole distributions have interpenetrated. The temporal decay of the EL at the end of the applied voltage pulse indicates the depletion of the carrier reservoir established during the preceding on-phase.

In this study, we aim to study the effects of TMIn treatment during growth interruption on the emission and carrier transport characteristics of InGaN green LEDs. EL, QE, and TREL measurements are conducted to determine the radiative decay and nonradiative decay rates. The resulting recombination dynamics are correlated with the device characteristic, carrier transport behavior, and efficiency droop of the TMIn-treated LEDs.

This paper is organized as follows: In section 2, sample structures and experimental procedures are described. In section 3, experimental results and discussions are reported. Finally, conclusions will be drawn in section 4.

Sample Structures and Experimental Procedures

The samples were grown on *c*-sapphire by low-pressure MOVPE. Ammonia (NH_3), trimethylgallium, triethylgallium, TMIn, trimethylaluminum, biscyclopentadienil (Cp_2Mg), and disilane (Si_2H_6) were

* Electrochemical Society Active Member.
z E-mail: swfeng@nuk.edu.tw

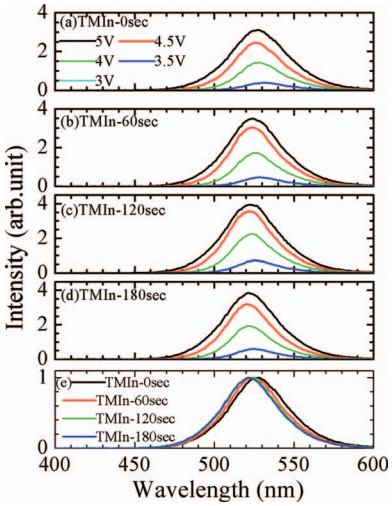

Figure 1. EL spectra at room temperature for (a) TMIn-0 sec, (b) TMIn-60 sec, (c) TMIn-120 sec, and (d) TMIn-180 sec LEDs. (e) Normalized EL spectra with a 5 V applied voltage for the four samples.

used as the precursors and dopants. The LED structures consisted of a 30 nm GaN nucleation layer, 1.5 μm GaN buffer layer, a 2.5 μm *n*-GaN contact layer, and five InGaN(3 nm)/GaN(15 nm) QWs, a 10 nm *p*-AlGaN, and an 0.2 μm *p*-GaN. The growth temperatures of QWs and *p*-layers are 780°C and 1,000°C, respectively. Indium tin oxide (300 nm) and Ti-Al (20/500 nm) were the ohmic contacts to *p*-type and *n*-type GaN, respectively. The LEDs had a mesa structure with an area of 350×350 μm. For the TMIn treatment process, an extra step with only TMIn and NH_3 flowing into the reactor was introduced at each InGaN-to-GaN interface during the growth of the MQWs. TMIn treatment times for the TMIn-60 sec, TMIn-120 sec, and TMIn-180 sec LEDs were 60, 120, and 180 seconds, respectively. One LED sample (TMIn-0sec) without TMIn treatment was also prepared as a control. The details of growth procedure and device preparation were described in a previous study.[11,12]

Current-voltage (*I-V*) characteristics were measured with a semiconductor parameter analyzer (Agilent 4145B). For electroluminescence (EL) spectrum and luminescence efficiency measurements, the LED devices were placed in an integrating sphere. A power supply was used to apply voltage to the LED devices. The luminescence from each LED sample was collected by the integrating sphere and focused into a spectrometer with a USB interface (Ocean Optics, resolution 0.3 nm). In addition, for TREL measurements, a pulse generator (Agilent 81110A) was used to generate voltage pulses to the devices. The repetition rate and width of the pulse were 1 kHz and 1 μs, respectively. The light output was detected by a fast-biased silicon photodiode (Electro-Optics Technology Inc., model ET-2020) operating directly on the surface of each device. The temporal evolution of the EL signals was recorded by a digital oscilloscope (Agilent, model DSO 6052A, 500 MHz/4Gs/s). The overall resolution of the TREL system can be less than 400 ps. All the measurements were carried out at room temperature. The detailed measurement was described in our previous study.[15]

Experimental Results

Static electroluminescence (EL), I-V characteristics, and luminescence efficiency measurements.— Fig. 1 shows the EL spectra at room temperature for LEDs (a) TMIn-0 sec, (b) TMIn-60 sec, (c) TMIn-120 sec, and (d) TMIn-180 sec. Both a higher applied voltage and a longer TMIn treatment time were tested separately. With both, EL intensities are stronger. This shows that TMIn treatment enhances luminescence intensity. As the applied voltage increases, the peak positions of the four samples are all slightly blue-shifted,

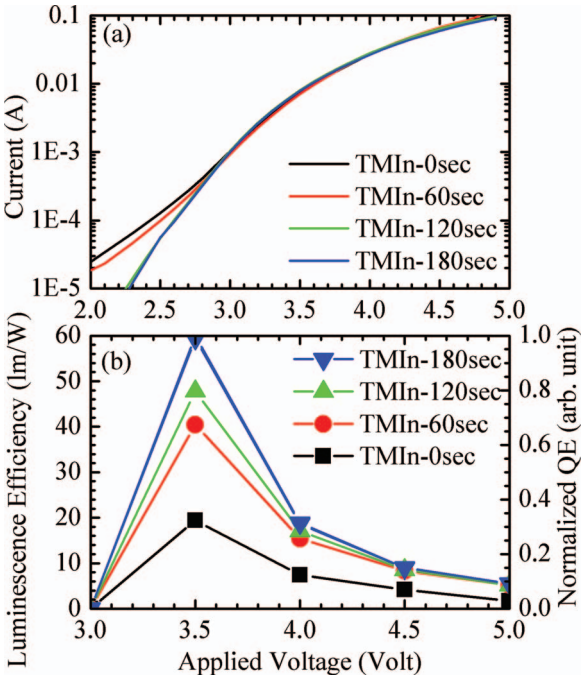

Figure 2. (a) Current density versus applied voltage (*I-V* curve) characteristics for the four samples. (b) Luminescence efficiency (left coordinate) and normalized quantum efficiency (right coordinate) as functions of applied voltage for the four LEDs.

as a result of a weaker QCSE.[16–19] In addition, Fig. 1e shows the normalized EL spectra with a 5 V applied voltage for the four samples. It is observed that as TMIn treatment time increases, the peak positions are slightly blue-shifted, but the spectral width slightly decreases. It has been reported that as the growth interruption time between the growth of the InGaN well and the GaN barrier increases, the emission peak of MQWs apparently blue-shifts due to indium desorption and strain relaxation.[4–6] With TMIn treatment during the growth interruption between InGaN well and GaN barrier, the indium vapor pressure prevents indium desorption and indium-rich clusters were removed by internal diffusion.[11,12] Indium composition becomes homogeneous inside the quantum well regions so that a lower V-shaped defect density, surface smoothing process, and better quantum well structure are obtained. Hence, as TMIn treatment time increases, the peak positions for the four samples are slightly blue-shifted. A less fluctuated potential energy results in a narrower spectral width and better color purity. Because of the EL peak position being slightly blue-shifted, the QCSE is not reduced in the TMIn-treated samples.

Fig. 2a shows the current versus applied voltage (*I-V*) characteristics of the four samples. Compared with the TMIn-untreated sample, the TMIn-treated samples (except for the TMIn-180 sec sample) show nearly the same operational threshold and a slightly larger slope of current versus applied voltage. This suggests that TMIn treatment doesn't change much the current, but enhances the recombination efficiency inside the active region. The 180sec-treated sample shows a slightly lower current for a voltage higher than 3.7 V, indicating that slight phase separation and indium aggregation may trap carriers and decrease the current density.

Fig. 2b shows the luminescence efficiency for the four samples. As the applied voltage increases, the luminescence efficiency first increases and then decreases. This is a well-known phenomenon, called "efficiency droop effect." Several arguments for efficiency droop have been proposed: polarization field,[16–19] carrier leakage at high forward currents,[20,21] Auger recombination,[22] junction heating,[23] and carrier delocalization from In-rich regions at high carrier densities.[24] It is observed that TMIn treatment can improve the luminescence efficiency.

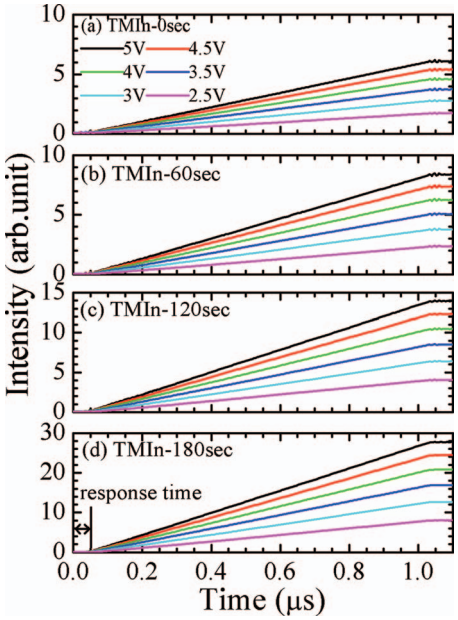

Figure 3. TREL rising profiles with pulse width 1μs for (a) TMIn-0 sec, (b) TMIn-60 sec, (c) TMIn-120 sec, and (d) TMIn-180 sec LEDs.

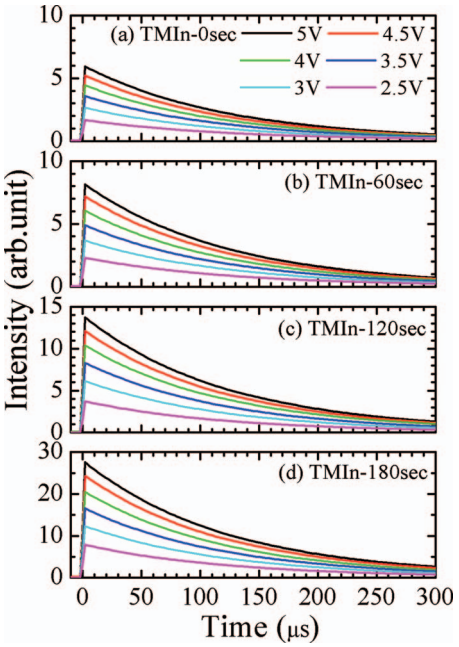

Figure 5. TREL decay profiles with pulse width 1μs for (a) TMIn-0 sec, (b) TMIn-60 sec, (c) TMIn-120 sec, and (d) TMIn-180 sec LEDs.

Carrier Transport Studies: TREL Measurement

In order to understand the operation mechanisms of InGaN green LEDs with TMIn treatment, TREL measurements were conducted. Fig. 3 shows TREL rising profiles with pulse width 1 μs for the four samples. With a larger applied voltage, the profiles rise more steeply and the response time is shorter. The intensity becomes stronger for the sample with a longer TMIn treatment time. In addition, Fig. 4 shows the response time as a function of applied voltage for the four samples. Response time $\tau_{response}$ can be described as the sum of carrier injection time, carrier transport time, and carrier relaxation time:

$$\tau_{response} = \tau_{injection} + \tau_{transport} + \tau_{relaxation} \quad [1]$$

where $\tau_{injection}$ is the carrier injection time to the Ohmic contact, $\tau_{transport}$ is the carrier transport time from the Ohmic contact to the active region, and $\tau_{relaxation}$ is the carrier relaxation time from the active region to the quantum well. As the applied voltage increases, the response time delay becomes shorter. A larger forward bias is beneficial for carrier injection, carrier drift velocity, and carrier transport such that hole and electron leading fronts meet faster and more easily. In addition, the TMIn-180 sec LED exhibits the shortest response time among the four samples. With the same device structure for the four samples, $\tau_{injection}$ and $\tau_{transport}$ are assumed to be the same.[1] Hence, the shorter response times of the TMIn-180 sec LED suggest that a better quantum well structure and reduced V-shaped defect density help carrier relaxation into the quantum wells and that a slight carrier localization helps carrier recombination, leading to a steeply increasing luminescence efficiency with a smaller applied voltage before reaching the maximum luminescence efficiency, as shown in the Fig. 2b.

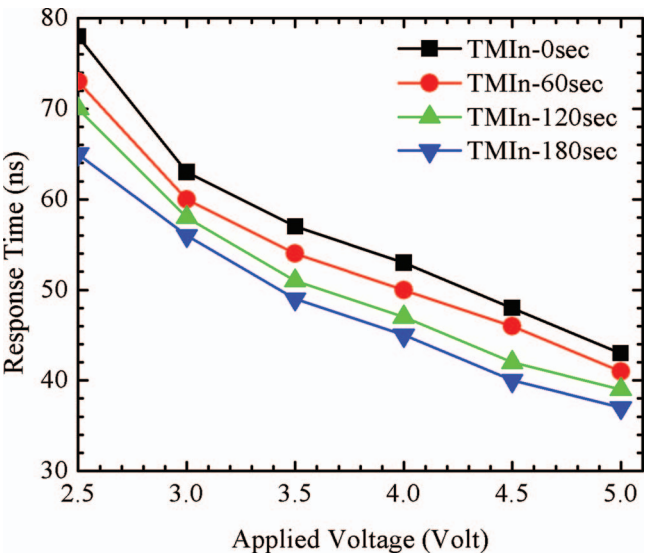

Figure 4. Response time as a function of applied voltage for the four LEDs.

Fig. 5 shows TREL decay profiles with pulse width 1 μs for the four samples. As applied voltage increases, the intensity becomes stronger. The EL decay can be fitted with a single exponential to obtain the decay time. Fig. 6a shows decay time as a function of applied voltage for the four samples. The shortest decay time of the TMIn-180 sec LED may suggest a fast radiative decay rate. It is noted that the time scale of response time is in the *ns* range while that of decay time is in the μ*s* range. This shows that carrier injection and carrier transport are efficient while carrier recombination in the active region is inefficient. As the applied voltage increases, the decay time decreases. Because of the slightly weaker QCSE at a larger applied voltage, the decreasing decay time can be explained with the slightly increasing overlap integral of electron and hole wavefunctions.[16–19] In addition, the decay time (τ) is the reciprocal of the decay rate ($\kappa = 1/\tau$). Fig. 6b shows the decay rate as a function of applied voltage for the four samples. The faster decay rate of the TMIn-180 sec LED may suggest a fast radiative decay rate. The measured decay rate is the sum of the radiative decay rate and nonradiative decay rate by the following equation 1:

$$\kappa = \kappa_r + \kappa_{nr} = \frac{1}{\tau} \quad [2]$$

where κ, κ_r, and κ_{nr}, and are the total decay rate, radiative decay rate, and nonradiative decay rate, respectively.

As shown in Figure 2b, the luminescence efficiency was normalized at the maximum efficiency (3.5 volt) of the TMIn-180 sec LED

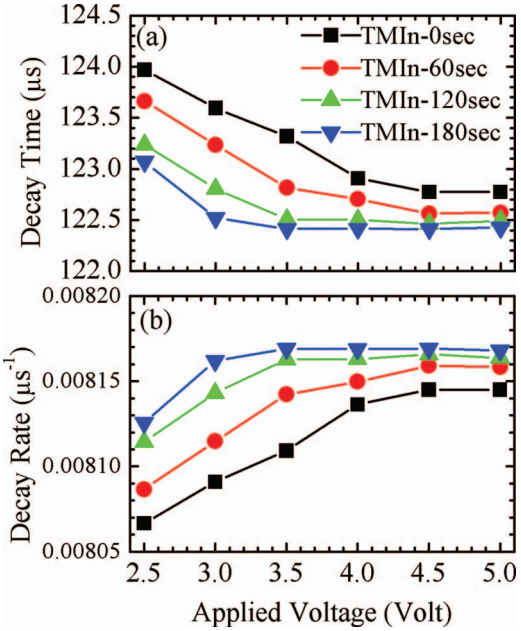

Figure 6. (a) Decay time and (b) decay rate as functions of applied voltage for the four LEDs.

to get the normalized quantum efficiency. Due to the same device structures, the extraction efficiencies of the four LEDs are assumed to be the same and the normalized quantum efficiency can be regarded as the internal quantum efficiency.[25] The internal quantum efficiency, η, is defined as the ratio of the number of light quanta emitted inside the device to the number of charge quanta undergoing recombination. η is described by the radiative decay rate over the total decay rate of recombination.[1] Hence, η can be expressed as

$$\eta = \frac{\kappa_r}{\kappa_r + \kappa_{nr}} = \frac{\kappa_r}{\kappa}. \qquad [3]$$

In order to quantitatively study the recombination dynamics, the observed decay rate (κ) and internal quantum efficiency (η) can be used to trace out the κ_r and κ_{nr} by solving equations 2 and 3.

κ_r and κ_{nr} associated with recombination dynamics are shown in Figure 7. κ_r exhibits a decreasing trend with increasing the applied voltage while κ_{nr} does the opposite. With the applied voltage 3.5 volt, the larger κ_r implies a better luminescence efficiency. At forward bias larger than 4 volt, the slower κ_r and fast κ_{nr} are responsible for the

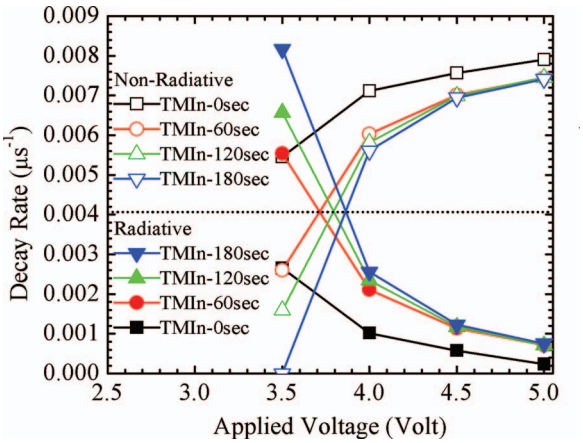

Figure 7. κ_r (filled symbol) and κ_{nr} (unfilled symbol) as functions of applied voltage for the four LEDs. Dotted line represents equal κ_r and κ_{nr}.

lower luminescence efficiency of the LED devices. The trends of κ_r and κ_{nr} can explain the efficiency droop effect for the four LEDs, as shown in Fig. 2b. As the TMIn treatment time increases, κ_r is enhanced while κ_{nr} becomes slower. This suggests that TMIn treatment leads to more homogeneous indium composition, less V-shaped defect density, and better quantum well structure such that luminescence efficiency is enhanced. For the TMIn-180 sec LED, the fastest κ_r and the slowest κ_{nr} suggest the strongest radiative recombination and best luminescence efficiency among the three TMIn-treated LEDs. In addition, it was found that κ_r and κ_{nr} are equal at $\sim 0.004\ \mu s^{-1}$ for the three TMIn-treated LEDs. The applied voltages $V_{\kappa_r=\kappa_{nr}}$, corresponding to equal κ_r and κ_{nr}, are ~3.7, ~3.8, and ~3.9 volts for the TMIn-60 sec, TMIn-120 sec, and TMIn-180 sec LEDs, respectively. The longer the TMIn treatment time, the larger the applied voltage $V_{\kappa_r=\kappa_{nr}}$. These demonstrate that the TMIn-180 sec LED exhibits the best luminescence efficiency among the TMIn-treated LED at all applied voltages. The resulting recombination dynamics are correlated with the device characteristics and performance of the TMIn-treated LEDs.

Discussion and Carrier Transport Characteristic Association with the Efficiency Droop Effect

The high-temperature growth of *p*-AlGaN and *p*-GaN layers may cause thermal degradation of the QWs, but this depends on the quality of the underlining QW layers. Without TMIn treatment, indium aggregation, phase separation, and high densities of threading dislocations and stacking faults lead to a poor quality QW. The depositions of *p*-AlGaN and *p*-GaN layers on the underlining QW layers show a rough surface morphology and poor sample quality. The high-temperature growth of *p*-AlGaN and *p*-GaN layers would cause thermal degradation of the QWs. On the other hand, with TMIn treatment, the deposition of *p*-AlGaN and *p*-GaN layers on the good quality QWs leads to a smoother surface morphology and better sample quality. The high-temperature growth of *p*-AlGaN and *p*-GaN layers may not cause a thermal degradation of the QWs.

We discuss the issues of carrier leakage by defect-related tunneling, polarization field, carrier delocalization, and Auger recombination to explain the efficiency droop in the TMIn-treated samples.

(I) The issue of carrier leakage by defect-related tunneling: the efficiency droop is due to the inefficient injection efficiency caused by excess tunneling current from QWs to defect-related states in the *p*-AlGaN barrier, and due to the reduced internal quantum efficiency due to tunneling of localized carriers in QWs to defect-related states in the *p*-AlGaN barrier.[20,21] For the TMIn-treated samples:

(i) for low applied voltages, $V < V_{max}$: the faster increasing efficiency with applied voltage for the TMIn-180 sec sample shows that lower defect-related states in the *p*-AlGaN barrier is beneficial to carrier injection into QWs. This argument is consistent with the shortest response time of the TMIn-180 sec LED.

(ii) for high applied voltages, $V > V_{max}$: the external quantum efficiency droop is due to the reduced internal quantum efficiency caused by tunneling of localized carriers in QWs to defect-related states in the *p*-AlGaN barrier. As the TMIn treatment time increases, the better quantum efficiency for the longer-treated samples, in particular for the TMIn-180 sec LED, is due to lower defect-related states in the high-quality *p*-AlGaN barrier. However, carrier leakage by defect-related tunneling of the longest-treated sample should not result in such a large efficiency droop. There must be some other mechanisms.

(II) The issue of polarization field: the EL peak positions of the TMIn-treated samples change only a little compared to that of the untreated one. This implies that the polarization fields in the TMIn-untreated and -treated samples are nearly the same. Hence, the unreduced polarization field in the TMIn-treated samples leads to the efficiency droop.

(III) The issue of carrier delocalization: the fast increasing EQE at the small injection current is due to carrier localization. The efficiency

droop under high injection current is attributed to the delocalization of carriers, while further droop at a higher injection current is due mostly to the carrier leakage.[24] For the TMIn-treated samples:

(i) for low applied voltages, $V < V_{max}$: because of sight phase separation and indium aggregation in the TMIn-180 sec LED, a slight carrier localization helps carrier recombination, leading to a faster rate of increase and a higher peak value of EQE.
(ii) for high voltages, $V > V_{max}$: carrier-carrier scattering leads to carrier delocalization and hence the efficiency droop.

(IV) The issue of Auger recombination: the Auger recombination rate is Cn^3, where C is Auger coefficient and n is the carrier density.[22] Auger coefficient is proportional to $(k_BT/E_g)^{2/3}\exp(-E_g/k_BT)$, where E_g is the band gap, k_B is Bozeman constant, and T is temperature. The carrier density is proportional to $J\tau/d$, where J is the current density, τ is the carrier lifetime, and d is the QW thickness. The EL peak positions (Fig. 1), current density (Fig. 2), and QW thickness of the TMIn-treated samples are nearly the same compared to that of the untreated one. In our previous study, as the TMIn treatment time increases, the carrier lifetime of the green band are smaller.[12] Hence, the smaller carrier lifetime leads to a weaker Auger recombination and hence a weaker efficiency droop in the TMIn-treated samples.

Comprehensive effects in the TMIn-treated samples:

(i) for low applied voltages, $V < V_{max}$: a lower V-shaped density of the TMIn-180 sec sample is beneficial to carrier injection into QWs and a slight carrier localization helps carrier recombination such that a steep increasing luminescence efficiency is observed.
(ii) for high voltages, $V > V_{max}$: lower V-shaped defect density, un-reduced polarization field, carrier delocalization, and weaker Auger recombination in the TMIn-treated samples lead to the inevitable efficiency droop.

Conclusions

In summary, with TMIn treatment, a more homogeneous indium composition, a better quantum well structure, and less V-shaped defect density result in a slightly blue-shifted peak position, narrower spectrum width, and better luminescence efficiency. In addition, the *ns*-scale response time and μs-scale decay time show that carrier injection and carrier transport are efficient while carrier recombination in the active region is inefficient. The shorter response times of the longer TMIn-treated LED suggest that a lower V-shaped density is beneficial to carrier injection into the quantum wells and that a slight carrier localization helps carrier recombination. The lower V-shaped defect density, un-reduced polarization field, carrier delocalization, and weaker Auger recombination in the TMIn-treated samples lead to the inevitable efficiency droop. Those mechanisms lead to the observation that the longest-treated sample shows the best efficiency and most significant droop of all the samples. The resulting recombination dynamics are correlated with the device characteristics and efficiency droop of the TMIn-treated LEDs. The research results provide important information to solve the efficiency droop of LEDs.

Acknowledgments

This research was supported by the National Science Council, Taiwan, R.O.C., under grants NSC 98-3114-E-110-001, NSC 99-2112-M-390-002-MY3, and NSC 99-2515-S-390-001.

References

1. E. Fred Schubert, *Light-Emitting Diodes* (Cambridge, 2006).
2. C. Wetzel and T. Detchprohm, Compound Semiconductor, January/February 2009.
3. S. W. Feng, C. K. Yang, C. M. Lai, L. W. Tu, Q. Sun, and J. Han, *J. Phys. D: Appl. Phys.*, **44**, 375103 (2011).
4. S. Y. Kwon, H. J. Kim, H. Na, H. C. Seo, H. J. Kim, Y. Shin, Y. W. Kim, S. Yoon, H. J. Oh, C. Sone, Y. Park, Y. Sun, Y. H. Cho, and E. Yoon, *Phys. Stat. Sol. (c)*, **0**, 2830 (2003).
5. H. K. Cho, J. Y. Lee, N. Sharma, J. Humphreys, G. M. Yang, and C. S. Kim, *Phys. Stat. Sol. (b)*, **228**, 165 (2001).
6. N. H. Niu, H. B. Wang, J. P. Liu, N. X. Liu, Y. H. Xing, J. Han, J. Deng, and G. D. Shen, *Optoelectron. Lett.*, **3**, 15 (2007).
7. Y. S. Lin, K. J. Ma, C. Hsu, S. W. Feng, Y. C. Cheng, C. C. Liao, C. C. Yang, C. C. Chou, C. M. Lee, and J. I. Chyi, *Appl. Phys. Lett.*, **77**, 2988 (2000).
8. S. F. Chichibu, A. Uedono, T. Onuma, B. A. Haskell, A. Chakraborty, T. Koyama, P. T. Feni, S. Keller, S. P. Denbaars, J. S. Speck, U. K. Mishra, S. Nakamura, S. Yamaguchi, S. Kamiyama, H. Amano, I. Akasaki, J. Han, and T. Sota, *Nat. Mater.*, **5**, 810 (2006).
9. S. W. Feng, L. W. Tu, J. I. Chyi, and H. C. Wang, *Thin Solid Films*, **517**, 909 (2008).
10. T. Hino, S. Tomiya, T. Miyajima, K. Yanashima, S. Hashimoto, and M. Ikeda, *Appl. Phys. Lett.*, **76**, 3421 (2000).
11. H. C. Lin, R. S. Lin, and J. I. Chyi, *Appl. Phys. Lett.*, **92**, 161113 (2008).
12. S. W. Feng, H. C. Lin, J. I. Chyi, C. Y. Tsai, C. J. Huang, H. C. Wang, F. W. Yang, and Y. S. Lin, *Thin Solid Films*, **519**, 6092 (2011).
13. W. Brütting, H. Riel, T. Beierlein, and W. Riess, *J. Appl. Phys.*, **89**, 1704 (2001).
14. M. Ichikawa, J. Amagai, Y. Horiba, T. Koyama, and Y. Taniguchi, *J. Appl. Phys.*, **94**, 7796 (2003).
15. S. W. Feng, M. C. Shih, C. J. Huang, and C. T. Chung, *Thin Solid Films*, **517**, 2719 (2009).
16. Y. M. Park, J. K. Son, H. J. Chung, C. Sone, and Y. Park, *Appl. Phys. Lett.*, **95**, 231917 (2009).
17. K. S. Kim, J. H. Kim, Y. M. Park, S. J. Jung, Y. J. Park, and S. N. Cho, *Appl. Phys. Lett.*, **97**, 031113 (2010).
18. J. H. Son and J. L. Lee, *Appl. Phys. Lett.*, **97**, 032109 (2010).
19. A. David and M. J. Grundmann, *Appl. Phys. Lett.*, **97**, 031113 (2010).
20. N. I. Bochkareva, V. V. Voronenkov, R. I. Gorbunov, A. S. Zubrilov, Y. S. Lelikov, P. E. Latyshev, Y. T. Rebane, A. I. Tsyuk, and Y. G. Shreter, *Appl. Phys. Lett.*, **96**, 133502 (2010).
21. M. H. Kim, M. F. Schubert, Q. Dai, J. K. Kim, E. F. Schubert, J. Piprek, and Y. Park, *Appl. Phys. Lett.*, **91**, 183507 (2007).
22. M. Zhang, P. Bhattacharya, J. Singh, and J. Hinckley, *Appl. Phys. Lett.*, **95**, 201108 (2009).
23. A. A. Efremov, N. I. Bochkareva, R. I. Gorbunov, D. A. Larinovich, Yu. T. Rebane, D. V. Tarkhin, and Yu. G. Shreter, *Semiconductors*, **40**, 605 (2006).
24. J. X. Wang, L. Wang, W. Zhao, Z. B. Hao, and Y. Luo, *Appl. Phys. Lett.*, **97**, 201112 (2010).
25. S. L. Chuang, Chapter 10 in *Physics of Optoelectronic Devices* (John Wiely & Sons, England, 1995).